Helmholtz-Zentrum Dresden-Rossendorf (HZDR)

Shape change of biogenic elemental selenium nanomaterials decreases their colloidal stability

Jain, R.; Jordan, N.; Tsushima, S.; Hübner, R.; Weiss, S.; Lens, P.;

Perma-Link to Publication Repository of HZDR:

https://www.hzdr.de/publications/Publ-24406

Nano impact

Selenium is an important element for dietary needs and technological applications, however, it is toxic to aquatic ecosystem at 5 μg L^{-1}. Both biogenic elemental selenium nanospheres and nanorods are formed during the biological treatment of selenium-laden wastewaters and thus, are present in the effluent of the bioreactor. This study, for the first time, demonstrated that the colloidal stability of the selenium nanomaterials is dependent on their shape and consequently affecting their fate in the environment and bioremediation effectiveness. This study also highlights the role of extracellular polymeric substances in providing different colloidal stability to differently shaped selenium nanomaterials and thus threw light on the complexity of the interaction of large biomolecules with differently shaped nanomaterials.

1
2
3
4
5
6
7
8
9
10
11
12
13
14
15
16
17
18
19
20
21
22
23
24
25
26
27
28
29
30
31
32
33
34
35
36
37
38
39
40
41
42
43
44
45
46
47
48
49
50
51
52
53
54
55
56
57
58
59
60

Graphical Abstract

Reduction

Inhibition of growth

Rise in the global temperature

EPS capped Bio-Se Nanorods: Colloidally less stable

EPS capped BioSe-Nanospheres: Colloidally more stable

Selenite

BioSe-Nanorods with EPS

BioSe-Nanospheres with EPS

Lower BioSe-Nanorods concentration in surface waters

Shape change of biogenic elemental selenium nanomaterials decreases their colloidal stability

Rohan Jain[1*], Norbert Jordan[2], Satoru Tsushima[2], René Hübner[3], Stephan Weiss[2], Piet Lens[1,4]

[1]*Department of Chemistry and Bioengineering, Tampere University of Technology, Korkeakoulunkatu 10, FI-33720 Tampere, Finland*

[2]*Helmholtz-Zentrum Dresden - Rossendorf, Institute of Resource Ecology, Bautzner Landstraße 400, 01328 Dresden, Germany*

[3]*Helmholtz-Zentrum Dresden - Rossendorf, Institute of Ion Beam Physics and Materials Research, Bautzner Landstraße 400, 01328 Dresden, Germany*

[4]*UNESCO-IHE, Institute for Water Education, Westvest 7, 2611AX Delft, The Netherlands*

*Corresponding author:

Phone: +358 401981098, e-mail: rohanjain.iitd@gmail.com, mailto: Department of Chemistry and Bioengineering, Tampere University of Technology, Korkeakoulunkatu 10, FI-33720 Tampere, Finland

1
2
3   Abstract
4
5   Selenium is an important element for technology and dietary supplements but it is toxic at
6
7   slightly higher concentration. Thus, its removal from the wastewaters is important.
8
9   Microbial reduction of selenium oxyanions in thermophilic bioreactor (55 ^{o}C) removed
10
11   higher selenium when compared to the control mesophilic bioreactor (30 ^{o}C). This study
12
13   demonstrated that the better performance of the thermophilic bioreactor was due to the
14
15   better settling properties of biogenic elemental selenium nanorods (BioSe-Nanorods)
16
17   produced in thermophilic conditions compared to biogenic elemental selenium
18
19   nanospheres (BioSe-Nanospheres) produced in mesophilic conditions. The BioSe-
20
21   Nanorods were less colloidally stable than the extracellular polymeric substances (EPS)
22
23   capped BioSe-Nanospheres as demonstrated by the former's lesser negative zeta
24
25   potential values when exposed to elevated concentrations of NaCl and $CaCl_2$ as well as
26
27   better settling in different lake waters. The lower colloidal stability was due to a lesser
28
29   negative surface charge density of BioSe-Nanorods compared to BioSe-Nanospheres.
30
31   This study also argued that the EPS were the corona of BioSe-Nanorods as well. Further,
32
33   this study observed that the formation of BioSe-Nanorods proceeds via BioSe-
34
35   Nanospheres. This study demonstrates the importance of the shape of nanoparticles in
36
37   determining their bioremediation effectiveness and the fate in the environment.
38
39
40
41
42
43
44
45
46
47   Keywords: Surface charge density, ζ-potential, microbial reduction, selenium nanorods,
48
49   DFT
50
51
52
53
54
55
56
57
58
59
60

2

INTRODUCTION

Selenium is a double-edged sword element: on one hand it is essential for human health (40 µg day^{-1})[1], but at a 10 times higher concentration it is toxic (400 µg day^{-1})[2]. For aquatic organisms and birds, selenium concentrations of as low as 5 µg L^{-1} in the water phase lead to adverse effects on their health including mortality due to bioaccummulation.[3] Therefore, the United States Environmental Protection Agency has the recommended discharge limit of 5 µg L^{-1} for selenium laden wastewaters.[4] Microbial reduction of selenium oxyanions to biogenic elemental selenium is a promising technology for treatment of selenium laden wastewaters prior to their discharge.[5–7]

The biological reduction of selenium oxyanions in the mesophilic (temperature range of 25 - 37 ^{o}C) leads to the formation of red, (mostly) amorphous and always spherical biogenic elemental selenium nanoparticles (BioSe-Nanospheres) with a diameter of 50-300 nm[8–11]. These BioSe-Nanospheres are colloidally stable owning to a corona of extracellular polymeric substances (EPS) coating the elemental selenium particles.[8] The presence of this EPS corona leads to a higher mobility of the BioSe-Nanospheres, thus resulting in a higher total selenium concentration in the effluent of the bioreactor.[9] On the contrary, Dessí et al (2016)[12] showed that the reduction of selenate in a thermophilic bioreactor at 55 ^{o}C resulted in a lower total selenium concentration in the effluent compared to control bioreactor operated at 30 ^{o}C under similar conditions. Further, the study observed the formation of biogenic elemental selenium nanorods (BioSe-Nanorods) in the thermophilic bioreactor (55 ^{o}C), while BioSe-Nanospheres were formed in the control mesophilic bioreactor (30 ^{o}C). However, this study could not identify the reasons for the lower total selenium concentrations in the effluent of thermophilic bioreactor. The identification of this reason is important not only to improve the remediation effectiveness of the biological

3

treatment technology for selenium removal from wastewaters, but also to understand the fate of selenium nanomaterials in the environment.

This study hypothesized that the change in the shape of the biogenic elemental selenium nanomaterials from spheres to nanorods led to the change in their colloidal stability leading to their different settling properties. The shapes of the nanomaterials affects their interaction with the biomolecules including proteins, lipid bilayers and EPS[13–15], especially when the nanomaterials are in higher aspect shapes such as nanorods[16]. The differences in these interactions of biomolecules with nanomaterials (electrostatic, steric, and other forces) due to their shape affect the properties of the interacting biomolecule.[17] The changes in the structure and composition of the biomolecules upon interaction with the nanomaterials affect the properties of the corona present on the nanomaterials and consequently the properties of nanomaterials[18] leading to possibly different surface charge density and colloidal stability.

However, there are no different studies comparing the colloidal properties of BioSe-Nanospheres and BioSe-Nanorods. Further, the BioSe-Nanorods formation and their characterization was never carried out. Thus, prior to comparing the colloidal properties of BioSe-Nanorods and BioSe-Nanospheres, this study described the formation of BioSe-Nanorods as well as their surface characterization. The formation of BioSe-Nanorods during the microbial reduction of selenite by anaerobic granular sludge at 55 $^{\circ}$C was studied by means of Scanning Electron Microscopy coupled with Energy-Disperse X-ray Spectroscopy (SEM-EDXS), Raman Spectroscopy and Infrared Spectroscopy (FT-IR). The surface charge of BioSe-Nanorods was studied by acid-base titration and zetametry. Settling experiments and ζ-potential measurements were carried out for both BioSe-

Nanorods and BioSe-Nanospheres. To gain insights into the interaction between biomolecules and nano-selenium, density functional theory (DFT) calculations were performed on clusters of Se_8 ring proxies for BioSe-Nanospheres and Se_8 helical selenium chains as proxies for BioSe-Nanorods to determine the charge distribution on selenium clusters.

EXPERIMENTAL

BioSe-Nanospheres and BioSe-Nanorods production and purification

BioSe-Nanospheres and BioSe-Nanorods were produced by the reduction of selenite in the presence of anaerobic granular sludge under anaerobic conditions at, respectively, 30[8] and 55 °C. The produced nanomaterials were purified as follow: the biomass was separated from the nanomaterials by decanting and centrifugation at 3,000 g for 15 minutes. The collected supernatant was concentrated by centrifugation at 37,000 g followed by sonication and hexane separation.[8] The selenium concentration in the BioSe-Nanospheres and BioSe-Nanorods was measured by ICP-MS as described in Jain et al. (2015).[8]

Characterization of BioSe-Nanorods

Transmission electron microscopy (TEM) analyses and IR spectroscopy measurements were carried out after the purification of BioSe-Nanorods. After 4 times concentrating the selenium nanomaterial present in the incubation bottles without purification (Figure 1a - 1f), time-dependent SEM-EDXS and Raman spectroscopy measurements were carried out. XRD of BioSe-Nanorods was carried out by drying the purified BioSe-Nanorods at room temperature and grinding the powder before the measurements. ζ-potential versus

5

pH profiles and acid-base titrations of BioSe-Nanorods were carried out at selenium concentrations of 16.5 mg L^{-1} and 163.4 mg L^{-1}, respectively.

Experiments on the colloidal stability of BioSe-Nanospheres and BioSe-Nanorods

The final concentration of BioSe-Nanospheres and BioSe-Nanorods used for the measurement of the ζ-potential when exposed to the increasing NaCl and CaCl$_2$ concentrations was 10 mg L^{-1}. The starting pH of both the BioSe-Nanospheres and BioSe-Nanorods was 7.3 (± 0.2). 2.5 mL of selenium nanomaterial was mixed with different concentrations and volumes of NaCl and CaCl$_2$ to achieve the desired salt concentrations. The final volume was made to 3.0 mL after adding MQ water, if required. The equilibrium pH was not controlled so as not to interfere in the reaction between the selenium nanomaterials and the salts.

Settling experiments of BioSe-Nanospheres and BioSe-Nanorods

The neutral lake water, acidic lake water and seawater were artificially prepared by mixing different salts at different concentrations as described in earlier studies.[19–21] The pH of acidic lake water, neutral lake water and sea water was, respectively, 5.0, 8.6 and 7.9. 5 mL of BioSe-Nanospheres and BioSe-Nanorods solution was prepared and the pH was adjusted to 7.3 (± 0.2), if required. These 5 mL selenium nanomaterial suspension were mixed with 55 mL of artificial waters so that the final concentration of selenium in the waters was 10 mg L^{-1}. The mixture of selenium nanomaterial and artificial waters was sonicated (5 min at 23 kHz). The mixture was then poured in 25 mL identical glass cylinders. The settling experiments were carried out for 24 h. At the end of 24 h, 0.5 mL of the sample was collected from the top 1 cm layer of the suspension. The experiment was

carried out in duplicates and if the difference was higher than 10%, then the whole experiment was repeated. The ζ-potential of the mixture was also measured.

DFT calculations

The calculations were performed with the Gaussian 09 suite of programs[22] at the B3LYP level[23] using double-zeta all-electron basis sets on Se[24]. Calculations were performed in the gas phase and the NBO version 3.1 in Gaussian 09 was used for natural bond orbital analysis, which include 4s 4p in the valence.

Analytics

SEM-EDXS, Infrared spectroscopy, ICP-MS, ζ-potential measurements and acid-base titrations were performed as described previously.[8,25] Raman measurements were performed at room temperature with a HORIBA LabRam ARAMIS Raman spectrometer equipped with a CCD detector (Nd-YAG laser, excitation wavelength 532 nm, P = 50 mW). Spectra were averaged out of 256 scans. TEM investigations were performed using an image-corrected Titan 80-300 microscope (FEI). To reveal the phase information of the selenium nanoparticles, selected SAED patterns were recorded and modeled with the software package JEMS. Prior to each TEM analysis, the specimen mounted in a double-tilt analytical holder was placed for 10 s into a Model 1020 Plasma Cleaner (Fischione). XRD analysis was carried out on a Bruker D8 Advance diffractometer as described in an earlier study.[26]

RESULTS

Formation of BioSe-Nanorods

SEM images obtained during the course of the reduction of selenite to elemental selenium by anaerobic granular sludge at 55 $^{\circ}$C show that the formation of BioSe-Nanorods is mediated through elemental selenium nanospheres which were observed transiently after 18 h of incubation. Their sizes varied between 50 and 300 nm in diameter (Figure 1a). After 24 h and 39 h of incubation, a growing number of BioSe-Nanorods was detected (Figures 1a), while at 48 h and 120 h of incubation, mainly BioSe-Nanorods were present (Figures 1a). The SEM and transmission electron microscopy (TEM) analyses showed that the length to diameter ratio of the purified BioSe-Nanorods exceeds 20: they have diameters between 20 and 50 nm and lengths between 300 and 700 nm with a median of 570 nm (Figures S1a, S1b and S1f). EDXS analyses in the SEM confirmed that the BioSe-Nanorods are mainly composed of selenium (Figure S2). In addition, carbon, oxygen, sulfur, and phosphorous are present (Figure S2). The detection of iron can be attributed to remnants of the inoculum anaerobic granular sludge. The produced BioSe-Nanorods were similar to chemically synthesized selenium nanorods (CheSe-Nanorods) regarding their size distribution (Figure 1a).
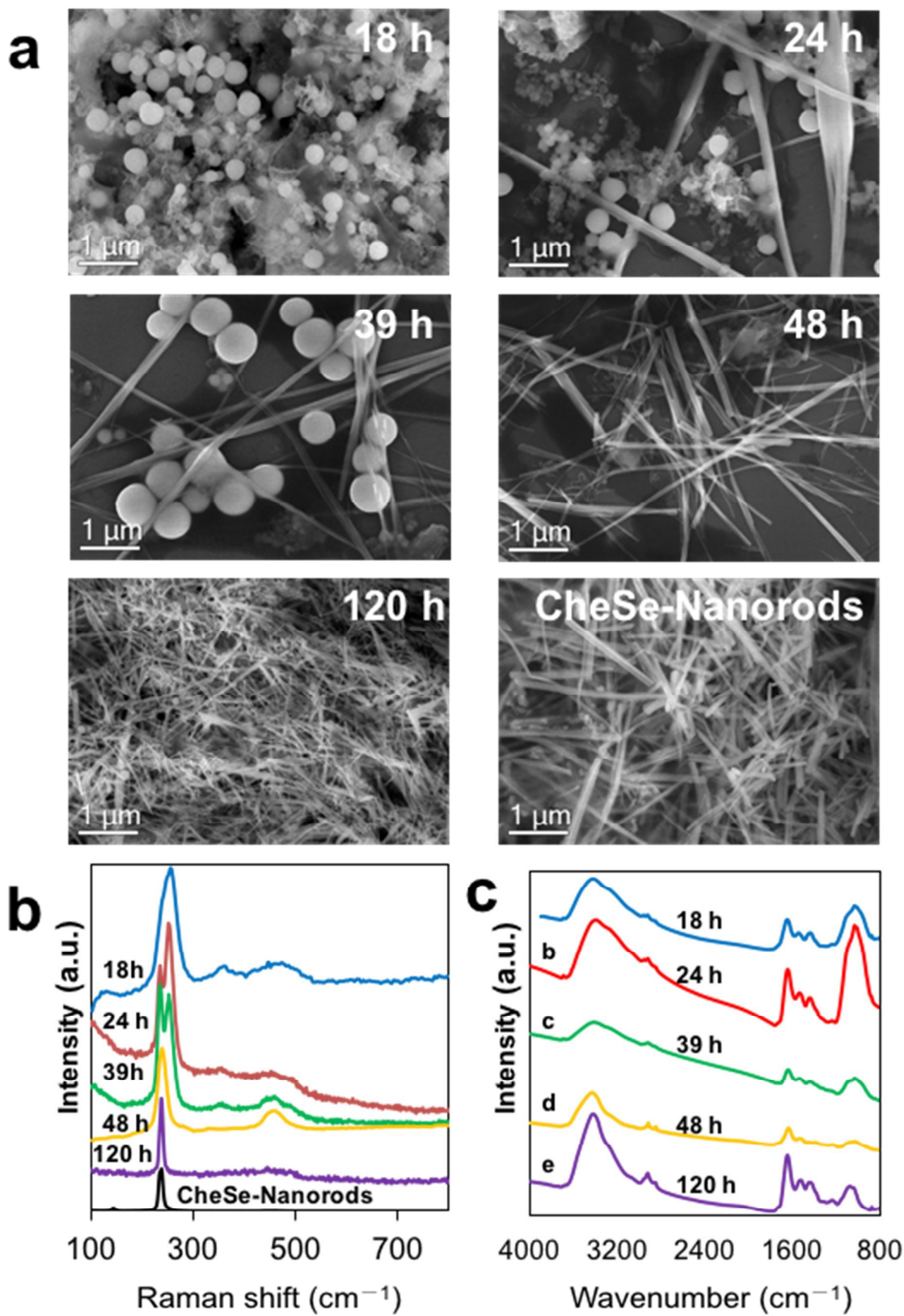
Figure 1. (a) SEM images of BioSe-Nanorods formed by biological reduction of selenite at 55 $^{\circ}$C and recorded after 18 h, 24 h, 39 h, 48 h and 120 h of incubation as well as SEM image of chemically synthesized selenium nanorods (CheSe-Nanorods) formed by the reduction of selenite by glutathione (reduced) in the absence of EPS. (b) Raman spectra and (c) corresponding IR spectra of the BioSe-Nanorods samples after different hours of incubation and Raman spectra of the CheSe-Nanorods. Note that the IR spectrum of CheSe-Nanorods was not recorded as no capping agent is added to this reaction.

Characteristics of BioSe-Nanorods

Selected area electron diffraction (SAED) in the TEM confirms the crystalline nature of the BioSe-Nanorods (Figure S1c). In particular, the single-crystalline diffraction pattern of the large BioSe-Nanorod shown in the inset of Figure S1c can be modeled using the trigonal phase of selenium (space group $P3_121$), with the c-axis of the hexagonal setting pointing in axial rod direction. CheSe-Nanorods have the same structure. Besides a few weak reflections of a secondary phase, the ring-type SAED pattern of an ensemble of CheSe-Nanorods is also described by trigonal selenium (Figure S1d). The BioSe-Nanorods and CheSe-Nanorods show comparable XRD patterns (Figure S1e). All diffraction maxima can be indexed with the trigonal phase of selenium.[27]

The Raman spectra of the 18 h incubated samples showed a feature at 253 cm^{-1}, which is a characteristic peak of amorphous selenium arising from intrachain bond-stretching vibrational mode, attributed to the disordered selenium chains with a minor contribution of the Se$_8$ rings[28–30] (Figure 1b).[30,31] Note that the minor contribution of Se$_8$ rings was attributed as a low intensity shoulder at ~260 cm^{-1}.[30,31] The shoulder at ~235 cm^{-1} already present after 18h of incubation and clearly visible after 24h is due to the intrachain

bond-stretching vibrational mode of the chains having a trigonal selenium like conformation.[29–31] After 48 and 120 h of incubation, the Raman spectra of the BioSe-Nanorods as well as of the CheSe-Nanorods showed the main feature at 237 cm^{-1}, characteristic of the trigonal allotropic form of elemental selenium arising from the vibration of Se-helical chains (Figure 1b).[32] The peak observed at 237 cm^{-1} is in fact made of two Raman modes, namely the A_1 mode and the E'' mode, corresponding to symmetric and asymmetric breathing motion, respectively.[33] The increased feature of the band at 237 cm^{-1} (Figure 1b) with the incubation time from 18 h to 39 h reflects the crystallization of amorphous selenium to trigonal selenium.

IR spectra of the purified elemental selenium nanomaterials sampled after 18, 24, 39, 48 and 120 h of incubation at 55 ^{o}C show the presence of organic material mainly consist of proteins and carbohydrates (Figure 1c). The spectra confirmed the presence of O-H (3425 cm^{-1}) and N-H (3270 cm^{-1}) stretching vibrations from carboxylic and amine groups, respectively. The presence of aliphatic carbon chains (2962, 2925 and 2854 cm^{-1}) was confirmed by C-H vibrations. The small feature at 1735 cm^{-1} was attributed to the carboxylic groups. The presence of proteins was suggested by stretching vibrations of C=O (1646 cm^{-1}, amide I) and N-H (1519 cm^{-1}, amide II). Consequently, the band at 1236 cm^{-1} was attributed to stretching vibrations of C-N and bending N-H vibrations of the groups present in the proteins. The band at 1436 cm^{-1} can be attributed to carboxylic and/or methyl groups. A very small feature at 1315 cm^{-1} can be attributed to S-O stretching. The presence of carbohydrates was observed by the C-O-C and C-H (1073 - 1038 cm^{-1}) stretching vibrations. The presence of P=O was not observed. The features at 1646 cm^{-1} and broad feature between 1073 - 1038 cm^{-1} suggests the presence of proteins and carbohydrates on the BioSe-Nanorods, respectively.

11

Acid-base titrations were carried out to determine the pK_a values of various functional groups present on the surface of BioSe-Nanorods. The local minima in the derivative of the acid-base titration versus pH gives pK_a values of the various functional groups present on the surface of the BioSe-Nanorods (Figure 2), as described in an earlier study[8]. The local minima for the BioSe-Nanorods were observed at pH 7.4, 7.2, 5.4 and 3.3. The pK_a values observed at 7.4 and 7.2 can be attributed to sulfonic, sulfinic or thiol groups (Figure 2). The pKa values at 5.4 and 3.3 can be assigned to phosphoric or carboxylic acid groups and to carboxylic acid groups, respectively.
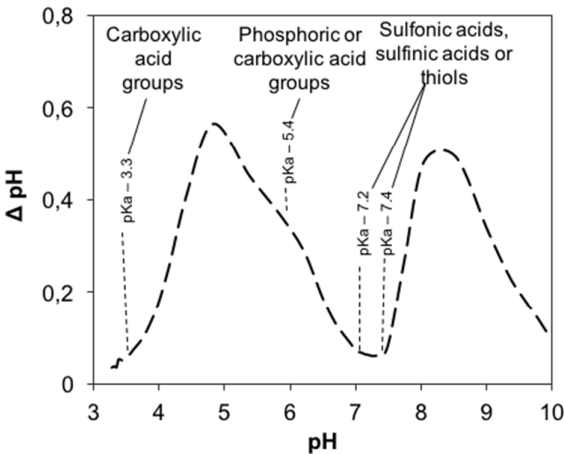

Figure 2. Derivative of acid-base titration data to identify the functional groups present on the surface of BioSe-Nanorods

The attached organics, forming the corona of the BioSe-Nanorods, provide them colloidal stability, as observed for the BioSe-Nanospheres as well.[8,9] The produced BioSe-Nanorods have a ζ-potential of −30.6 (± 0.8) mV and −21.9 (± 0.9) mV, respectively, at 1 mM and 10 mM NaCl, and at pH 7.3 (± 0.2) (Figure 3). The isoelectric point of the BioSe-Nanorods was observed at pH 3.2 and 2.8, respectively, for 1 mM and 10 mM NaCl. Note that the selenium concentration in the BioSe-Nanorods was 16.0 mg L^{-1} for ζ-potential measurements.
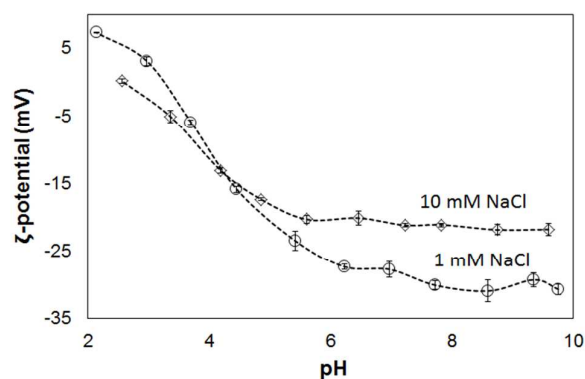
Figure 3. ζ-potential versus pH plot of BioSe-Nanorods at 1mM and 10 mM background NaCl concentration.

Comparing properties of BioSe-Nanorods with those of BioSe-Nanospheres

The colloidal stability of the BioSe-Nanorods (formed at 55 °C) and BioSe-Nanospheres (formed at 30 °C) was compared by means of ζ-potential measurements after dosing of equal amounts of NaCl and $CaCl_2$ in a 10 mg L^{-1} selenium concentration of BioSe-Nanospheres or BioSe-Nanorods. The addition of both NaCl and $CaCl_2$ led to a decrease of the ζ-potential of BioSe-Nanospheres and BioSe-Nanorods (Figure 4a and 4b). At 10 mM NaCl, the ζ-potential of the BioSe-Nanospheres changed from -34.2 ($\pm$ 0.4) mV to -32.7 ($\pm$ 1.5) mV, while that of the BioSe-Nanorods changed from -31.1 ($\pm$ 0.7) mV to -17.0 ($\pm$ 0.8) mV suggesting poorer colloidal stability of the BioSe-Nanorods with increasing ionic strength. Further, when the NaCl concentration was increased to 100 mM, the ζ-potential of the BioSe-Nanospheres and BioSe-Nanorods changed to, respectively, -17.9 ($\pm$ 1.0) mV and -7.9 ($\pm$ 0.9) mV. Similarly, at 10 mM $CaCl_2$, the ζ-potential of the BioSe-Nanospheres and BioSe-Nanorods, respectively, changed from -32.1 ($\pm$ 0.5) mV to -10.2 ($\pm$ 0.2) mV and -29.0 ($\pm$ 1.5) to -6.4 ($\pm$ 0.5) mV (Figure 4b).
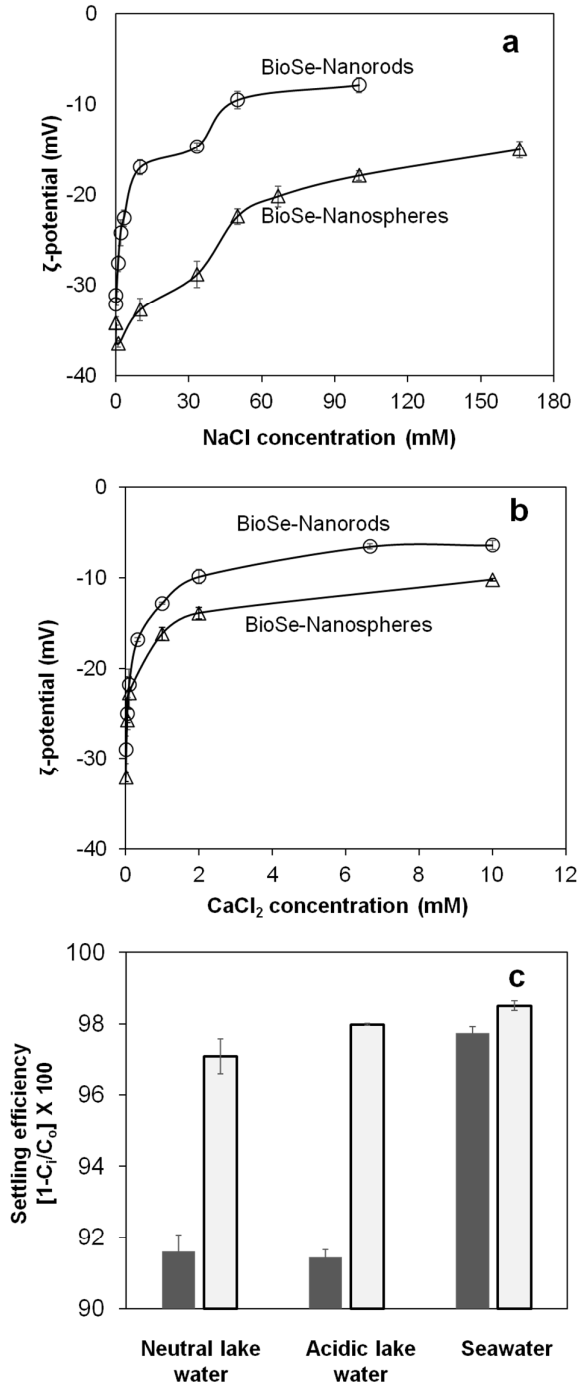
Figure 4. Variation in the ζ-potential of BioSe-Nanospheres (△) and BioSe-Nanorods (○) with the addition of (a) NaCl and (b) CaCl$_2$. (c) Settling efficiencies of BioSe-Nanospheres (■) and BioSe-Nanorods (□) in artificial lake water, acidic lake water and sea water. C$_i$ and C$_o$ denotes, respectively, the Se concentration in the top 1 cm layer of the settling cylinder at t = 24 h and initial Se concentration.

14

The BioSe-Nanospheres showed a 91.6 (± 0.5)% and 91.4 (± 0.2)% settling efficiency, respectively, in neutral lake water and acidic lake water after 24 h (Figure 4c). On the other hand, BioSe-Nanorods displayed a 97.1 (± 0.5)% and 98.0 (± 0.1)% settling efficiency, respectively, in neutral and acidic lake water. In the seawater, both BioSe-Nanospheres 97.8 (± 0.2)% and BioSe-Nanorods 98.5 (± 0.1)% revealed a similar settling efficiency (Figure 4c). The differences in settling efficiency of the BioSe-Nanospheres and BioSe-Nanorods in artificial acidic lake water and neutral lake water were also reflected in their ζ-potential values. In particular, the ζ-potential of BioSe-Nanospheres and BioSe-Nanorods in neutral lake water (Ionic strength: 3.6 mM, pH: 8.6 and divalent cations concentration: 0.4 mM) was, respectively, -21.9 (± 0.6) mV and -16.3 (± 0.4) mV. Similarly, the ζ-potential of the BioSe-Nanospheres and BioSe-Nanorods in acidic lake water (Ionic strength: 10.5 mM, pH: 5.0 and divalent cations concentration: 0.07 mM) was, respectively, -23.4 (± 0.5) mV and -17.5 (± 0.7) mV. In the artificial seawater, the ζ-potential of BioSe-Nanospheres and BioSe-Nanorods could not be recorded as the nanoparticles were settling too fast.

The surface charge density of BioSe-Nanospheres and BioSe-Nanorods was compared to explain the different colloidal stability of the BioSe-Nanospheres and BioSe-Nanorods. The number of H^+ moles adsorbed during the acid-base titration is an indirect, but accurate, comparison of the surface charge of the BioSe-Nanospheres and BioSe-Nanorods. Figure 5a shows the moles of H^+ adsorbed per g of selenium in the BioSe-Nanospheres were 7 times higher than those absorbed by the BioSe-Nanorods at pH 7.2. BioSe-Nanospheres consistently showed a higher H^+ adsorption capacity than BioSe-Nanorods throughout the tested pH range of 3.2 to 9.2 (Figure 5a). The adsorption of H^+ onto BioSe-Nanospheres decreases with increase of the pH in the bulk solution. The

derivative of H^+ moles adsorbed per g of adsorbent gives the buffering capacity of the adsorbent. As observed in Figure 5b, the BioSe-Nanospheres displayed a higher buffering capacity than BioSe-Nanorods between pH 3 and 10.
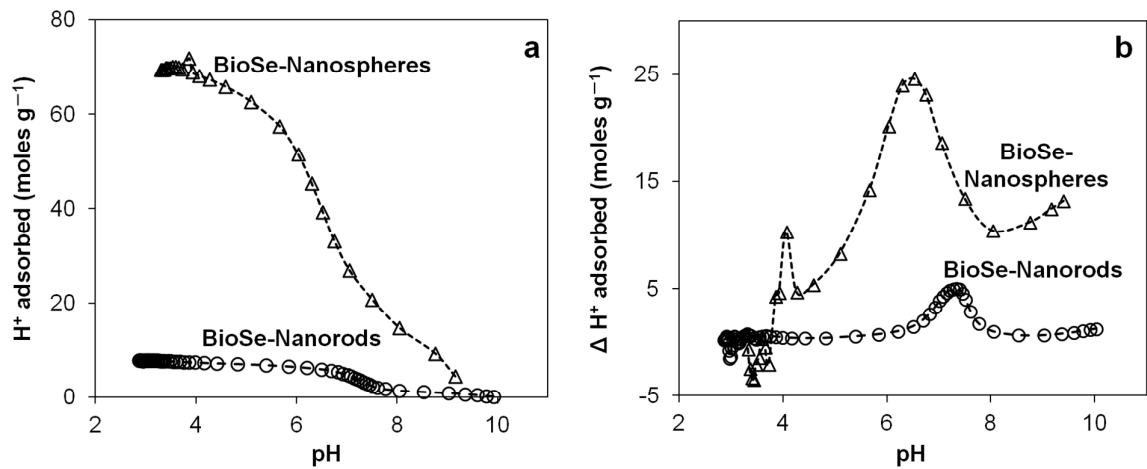

Figure 5. (a) Moles of H^+ adsorbed per unit Se mass in BioSe-Nanospheres (△) and BioSe-Nanorods (○) and (b) their corresponding derivative with respect to pH. Please note that the raw acid-base titration data of the BioSe-Nanospheres has been sourced from Jain et al. (2015).[8]

The different surface charge density of BioSe-Nanospheres and BioSe-Nanorods is also due to the differences in the interaction of biomolecules with elemental selenium, i.e. electrostatic and steric forces acting at different intensity on the nano-biomolecule interface. The electrostatic interaction of elemental selenium nanomaterials of different shapes and organics, such as EPS, depends on the charge distribution on the selenium clusters forming elemental selenium nanomaterials. The charge distribution on the selenium atoms in the selenium cluster depends on the structure of the selenium units forming the selenium cluster. The trigonal BioSe-Nanorods consist of Se_n helical chains arranged in $P3_121$ space groups (Figure 1b, Figure S1c, Figure S1e).[34] In contrast, the

forming units of amorphous BioSe-Nanospheres are not yet fully known[34] but are claimed

to consist of disordered selenium chains with a minor contribution of Se_8 rings. On the

other hand, chemically synthesized selenium nanospheres (CheSe-Nanospheres) in the

presence of the capping agents are spherical in shape, monoclinic in structure and their

forming units are Se_8 rings.[34,35] Further, Oremland et al. (2004)[36] have reported the

formation of monoclinic spherical selenium nanoparticles after biological reduction of

selenium oxyanions by *Sulfurospirillum barnesii*, *Bacillus selenitireducens*, and

Selenihalanaerobacter shriftii.[36] Thus, Se_8 rings of selenium arranged in P121 space

groups[34] were used as a proxy for the forming units of the amorphous BioSe-

Nanospheres.

To validate the hypothesis of a different charge distribution on selenium atoms due to

different forming units, DFT calculations and natural bond orbital (NBO) analysis of 96

selenium atoms arranged as Se_8 rings and Se_8 helical chains were carried out (Figure 6).

The charge distribution in the helical selenium chains varied from -0.275 to 0.185 e (Figure

6a), while in the Se_8 rings, the charge distribution varied from -0.046 to 0.021 e (Figure

6b). The edge selenium atoms in the helical chains displayed the highest positive charge

and the immediate neighboring atom to the edge was most negative. Since the selenium

edge atoms are deficient in bonds, there is less localization of electrons thereby 4p

occupation is slightly deficient (~ 3.8) than its formal configuration of $4p^4$, whereas the

neighboring atoms have excess 4p electrons (~ 4.3) (Figure 6a). The charge on the

central selenium atoms in the chain varied between -0.050 and 0.050 e, which is slightly

higher than the one observed in the Se_8 rings. Thus, as observed in Figure 6, the edge

charge on the helical chain is 5 times higher than that on the Se_8 rings.

1
2
3
4
5
6
7
8
9
10
11
12
13
14
15
16
17
18
19
20
21
22
23
24
25
26
27
28
29
30
31
32
33
34
35
36
37
38
39
40
41
42
43
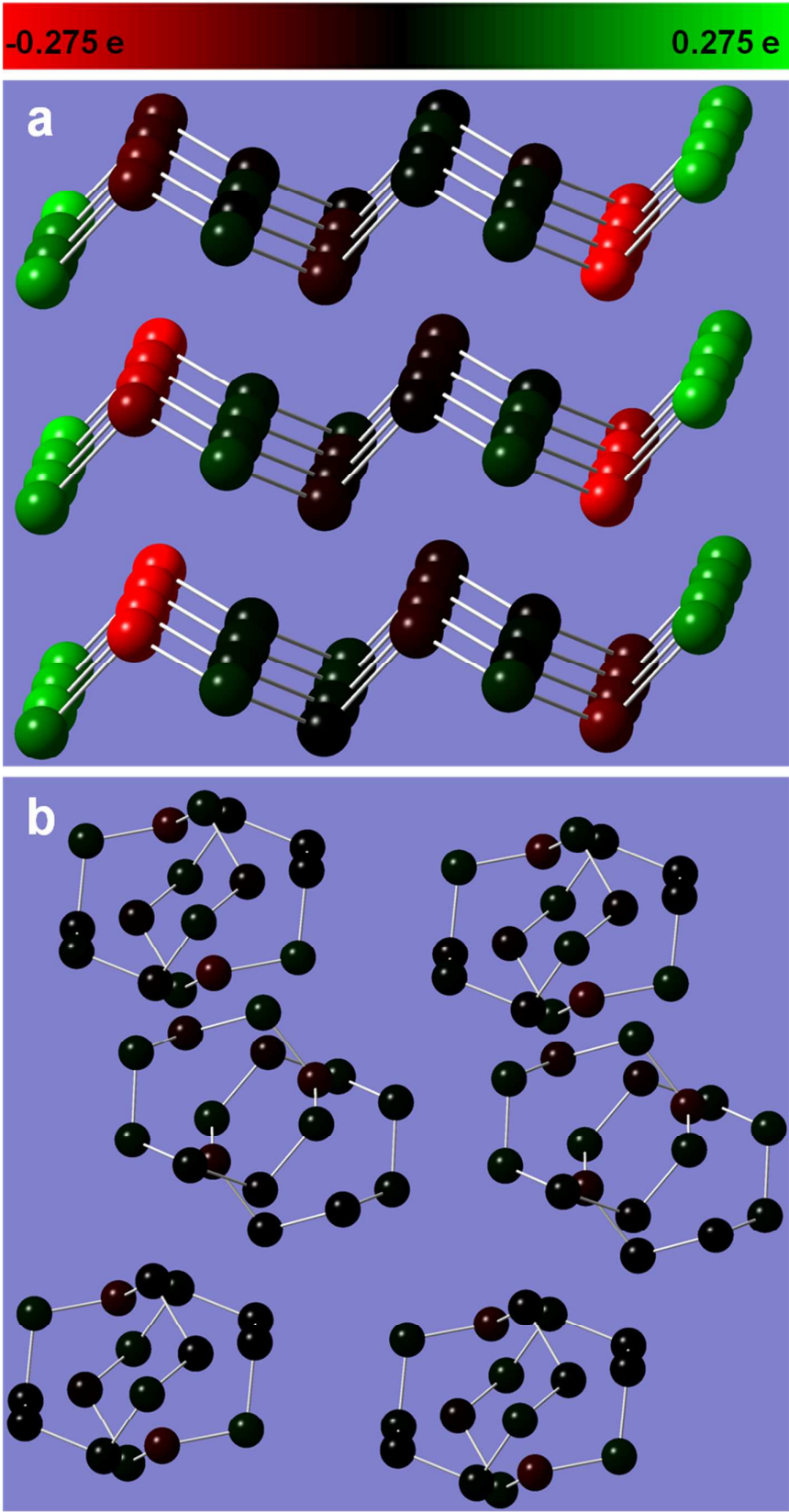44
45
46
47
48
49
50
51
52
53
54
55
56
57
58
59
60

Figure 6. Natural atomic charge distribution on the 96 selenium atoms arranged as (a) Se_8 helical chains and (b) Se_8 rings. Se_8 helical chains are the forming units of the BioSe-Nanorods, while the Se_8 rings are used as the proxy for the forming units of BioSe-Nanospheres. 96 selenium atoms is a reasonable sized cluster for determining charge distribution without exceeding computing limits.[37]

DISCUSSION

BioSe-Nanorods are colloidally less stable than the BioSe-Nanospheres

This is the first study that demonstrates that a change in shape of biogenic selenium nanomaterials from nanospheres to nanorods decreases their colloidal stability (Figure 4). The poorer colloidal stability of BioSe-Nanorods when compared to BioSe-Nanospheres is evident from the BioSe-Nanorods' less negative ζ-potential values when exposed to equal concentrations of NaCl and $CaCl_2$ (Figure 4a, 4b) or when mixed with acidic and neutral lake water (Neutral lake water: BioSe-Nanospheres -21.9 ± 0.6 mV and BioSe-Nanorods -16.3 ± 0.4 mV; Acidic lake water: BioSe-Nanospheres -23.4 ± 0.5 mV and BioSe-Nanorods -17.5 ± 0.7). The poorer stability was further evidenced by a better settling efficiency of the BioSe-Nanorods in acidic and neutral lake water (~97% compared to ~91% of BioSe-Nanospheres) (Figure 4c). It is interesting to note that the biogenic elemental selenium nanomaterials lost their colloidal stability at much lower divalent cation concentrations compared to monovalent cation concentrations. This was due to higher charge screening by divalent cations (Figure 4c). Similar phenomenon was also observed for the reduced graphene oxide nanoparticles.[38]

The lower colloidal stability of BioSe-Nanorods compared to BioSe-Nanospheres enhances the bioremediation effectiveness of bioreactors treating selenium containing

wastewater by skipping or minimizing the secondary treatment required for removal of colloidal elemental selenium.[9] Indeed, Dessi et al. (2016)[12] demonstrated that a thermophilic upflow anaerobic sludge blanket reactor operating at 55 ^{o}C had a lower total selenium effluent concentration compared to a control mesophilic upflow anaerobic sludge blanket reactor operating at 30 ^{o}C, even when the selenate reduction and selenium volatilization rates were similar. The present study demonstrated the better settling of such BioSe-Nanorods as one of the reasons for the better selenium removal performance of the thermophilic bioreactor.

This lower colloidal stability of BioSe-Nanorods than BioSe-Nanospheres implies that the former are less mobile in the environment. The difference of 6% in the settling efficiency, though small, corresponds to 600 µg L^{-1} more selenium in the top layer of the water column when the starting selenium concentration is 10 mg L^{-1}, typically found in surface water (CA, USA), gold-mines and lead mine wastewater, and Flue gas desulfurization process water[7]. Even if the starting selenium concentration is reduced to 500 µg L^{-1} (found in agricultural drainage wastewater)[7], this still correspond to a difference of 30 µg L^{-1}, which is 6 times the recommended discharge criterium of United States Environmental Protection Agency[4] and high enough for causing mortality of aquatic organisms[39].

The lower mobility of BioSe-Nanorods compared to BioSe-Nanospheres will also affect the environmental partitioning factor (K_d) determining the selenium distribution between the water (mobile) and sediment (stationary) phase.[40] This study threw light on the mobility of the biogenic elemental selenium nanomaterials in the environment and pinpointed the role of temperature in accurately determining K_d values to improve the accuracy of the biogeochemical models of selenium.

EPS is the corona of the BioSe-Nanorods

BioSe-Nanospheres are colloidally stabilized by a corona of EPS consisting mainly of proteins and carbohydrates.[8,9,41] It is also known that the EPS governs the surface properties of BioSe-Nanospheres.[8] This study demonstrated for the first time that the BioSe-Nanorods produced by anaerobic granular sludge were also colloidally stable due to a corona of organics containing both proteins and carbohydrates (Figure 1c). The organics attached to the BioSe-Nanorods originate from the EPS produced by the anaerobic granules. The ζ-potential versus pH profiles of EPS, EPS-capped chemically synthesized selenium nanospheres (EPS-capped CheSe-Nanospheres), and BioSe-Nanospheres with isoelectric points at 2.3, 2.8 and 3.2[8] are very similar to that (2.8 at 10 mM NaCl, Figure 3) of the BioSe-Nanorods. Further, features of the IR spectra of EPS, EPS-capped CheSe-Nanospheres and BioSe-Nanospheres are similar to that of BioSe-Nanorods (Figure 1c)[8]. The functional groups, determined by acid-base titration, present on the BioSe-Nanorods (Figure 2) are again very similar to the BioSe-Nanospheres produced by the same anaerobic granular sludge.[8] All the above confirms that the corona on BioSe-Nanorods is composed of EPS as well and determines their surface properties.

BioSe-Nanorods are colloidally stable due to the presence of EPS (Figure 3). This is in contrast to the CheSe-Nanorods produced by the reaction of selenite and glutathione (reduced) at ambient temperature (~25 $^{\circ}$C) in the absence of EPS.[8] The same chemical reaction when carried out in the presence of EPS leads to the formation of colloidally stable CheSe-Nanospheres.[8] Thus, EPS is providing colloidal stability to BioSe-Nanospheres, BioSe-Nanorods and EPS-capped CheSe-Nanospheres.

21

The corona on the BioSe-Nanospheres[8] and BioSe-Nanorods (Figure 1c, Figure 2 and Figure 3) consist of EPS, but their colloidal stability differs (Figure 4). This is due to the higher negative surface charge density of BioSe-Nanospheres compared to BioSe-Nanorods, indicated by a smaller amount of moles of H^+ adsorbed per unit mass of the selenium in the BioSe-Nanorods (Figure 5). The less negative ζ-potential of BioSe-Nanorods compared to BioSe-Nanospheres when exposed to NaCl and $CaCl_2$ (Figure 4a and 4b) is the result of the BioSe-Nanorods' lower surface charge density (Figure 5). The differences in the surface charge density of BioSe-Nanospheres and BioSe-Nanorods are also due to the differences in the interaction of nanorods and nanospheres with the EPS. The shape of the nanoparticles can change the properties of biomolecules upon their interaction[13] as observed during the interaction of BSA with nanorods and nanospheres of Au[17]. Indeed, the IR spectra of the BioSe-Nanospheres showed two features at 1460 and 1394 cm^{-1}, corresponding to carboxylic groups and/or methly groups, while the BioSe-Nanorods showed a single feature at 1436 cm^{-1} suggesting the variations in the interaction of carboxyl groups with BioSe-Nanospheres and BioSe-Nanorods. Moreover, different components of EPS at different scales interact with nanospheres and nanorods[13], thus affecting their surface properties. Further, the composition of EPS produced by anaerobic granules at 30 and 55 ^{o}C can vary[42], which further contributes to the different surface charge density of the BioSe-Nanospheres and BioSe-Nanorods.

The interaction of the EPS with the bare nano-selenium surface is mediated by different forces including electrostatic and steric forces.[14] The differences in the charge distribution of the helical chains (forming BioSe-Nanorods) and Se_8 ring clusters (proxy to BioSe-Nanospheres) (Figure 6), particularly at the edges of the helical chains, provide the fundamental basis of the electrostatic effect of the shape on the differences in the

interaction of the nano-selenium with the EPS. The lower radius of curvature of BioSe-Nanorods (12.5 nm orthogonal to the longitudinal axis) compared to BioSe-Nanospheres (median radius: 90 nm) leads to higher steric hindrance to the approaching EPS, thus leading to differences in the steric forces acting at the EPS and the bare nano-selenium interface. Thus, both electrostatic and steric forces, at different scales, are acting during the interaction of EPS and selenium nanospheres or nanorods, resulting in their different composition and properties of the corona and ultimately leading to a different surface charge density.

The reduction of selenite by glutathione (reduced) at ambient temperature (~25 ^{o}C) in the absence of EPS not only produces colloidally unstable selenium nanomaterials, but also produces a different phase of them when compared to selenite reduction in presence of EPS. Similarly, the reduction of selenite at 30 ^{o}C by anaerobic granular sludge produced BioSe-Nanospheres which are both colloidally stable as well as remain amorphous for more than 8 weeks.[36] This demonstrates that the EPS also provide phase stability at 30 ^{o}C. However, it is observed that at 55 ^{o}C, BioSe-Nanospheres capped with EPS (Figure 1a and 1c) were transformed to BioSe-Nanorods. This illustrates the limitation of EPS as stabilizing agent for the preservation of the spherical shape of the amorphous selenium nanoparticles at 55 ^{o}C. However, it continued to provide colloidal stability to the BioSe-Nanorods, albeit to a lower extent.

CONCLUSIONS

This study has demonstrated that the bioremediation effectiveness and the fate of selenium nanomaterials in the environment is strongly dependent on their shape. Furthermore, this study highlighted the effect of the nanomaterial shape on their

23

interaction with complex biomolecules such as EPS. These findings are even more interesting as the core (selenium in elemental form) and the corona (EPS) of BioSe-Nanospheres and BioSe-Nanorods are similar, but lead to a very different colloidal stability. These results suggest that the shape of the nanomaterials intrinsically affects their colloidal stability, which impacts their fate in the environment and bioremediation effectiveness.

REFERENCES
1   M. P. Rayman, *Lancet*, 2000, **356**, 233–41.
2   M. Lenz and P. N. L. Lens, *Sci. Total Environ.*, 2009, **407**, 3620–33.
3   S. J. Hamilton, *Ecotoxicol. Environ. Saf.*, 2003, **56**, 201–10.
4   US EPA, 2014, 2014.
5   A. W. Cantafio, K. D. Hagen, G. E. Lewis, T. L. Bledsoe, K. M. Nunan and J. M. Macy, *Appl. Environ. Microbiol.*, 1996, **62**, 3298–303.
6   A. B. Holmes and F. X. Gu, *Environ. Sci. Nano*, 2016, **3**, 982–996.
7   L. C. Tan, Y. V. Nancharaiah, E. D. van Hullebusch and P. N. L. Lens, *Biotechnol. Adv.*, 2016, **34**, 886–907.
8   R. Jain, N. Jordan, S. Weiss, H. Foerstendorf, K. Heim, R. Kacker, R. Hübner, H. Kramer, E. D. van Hullebusch, F. Farges and P. N. L. Lens, *Environ. Sci. Technol.*, 2015, **49**, 1713–1720.
9   B. Buchs, M. W. H. Evangelou, L. H. E. Winkel and M. Lenz, *Environ. Sci. Technol.*, 2013, **47**, 2401–2407.
10   R. Jain, G. Gonzalez-Gil, V. Singh, D. van Hullebusch, Eric, F. Farges and P. N. L. Lens, in *Nanobiotechnology*, eds. A. Kumar and N. Govil, J, Studium Press LLC, USA, 2014, pp. 361–390.

11   Y. V Nancharaiah and P. N. L. Lens, *MMBR*, 2015, **79**, 61–80.

12   P. Dessì, R. Jain, S. Singh, M. Seder-Colomina, E. D. van Hullebusch, E. R. Rene, S. Z. Ahammad, A. Carucci and P. N. L. Lens, *Water Res.*, 2016, **94**, 146–154.

13   M. P. Monopoli, C. Åberg, A. Salvati, K. A. Dawson, C. Aberg, A. Salvati and K. A. Dawson, *Nat. Nanotechnol.*, 2012, **7**, 779–786.

14   M. Mahmoudi, I. Lynch, M. R. Ejtehadi, M. P. Monopoli, F. B. Bombelli and S. Laurent, *Chem. Rev.*, 2011, **111**, 5610–5637.

15   K. Yang and Y.-Q. Ma, *Nat. Nanotechnol.*, 2010, **5**, 579–583.

16   R. M. Fratila, S. Rivera-Fernández and J. M. de la Fuente, *Nanoscale*, 2015, **7**, 8233–60.

17   S. Chakraborty, *Langmuir*, 2011, **27**, 7722–7731.

18   A. K. Suresh, D. A. Pelletier and M. J. Doktycz, *Nanoscale*, 2013, **5**, 463–474.

19   D. R. Kester, I. W. Duedall;, D. N. Pytkowicz, C. R. M. and R. M. Pytkowicz, *Limnol. Oceanogr.*, 1967, **12**, 176–179.

20   E. J. Smith, W. Davison and J. Hamilton-Taylor, *Water Res.*, 2002, **36**, 1286–1296.

21   T. Zotina, O. Koster and F. Juttner, *Freshw. Biol.*, 2003, **48**, 1859–1872.

22   M. J. Frisch, G. W. Trucks, H. B. Schlegel, G. E. Scuseria, M. A. Robb, J. R. Cheeseman, G. Scalmani, V. Barone, B. Mennucci, G. A. Petersson, H. Nakatsuji, M. Caricato, X. Li, H. P. Hratchian, A. F. Izmaylov, J. Bloino, G. Zheng, J. L. Sonnenberg, M. Had, Gaussian 09 Citation., 2009, Available at: http://www.gaussian.com/g_tech/g_ur/m_citation.htm.

23   C. Lee, W. Yang and R. G. Parr, *Phys. Rev. B*, 1988, **37**, 785–789.

24   N. B. Balabanov and K. A. Peterson, *J. Chem. Phys.*, 2005, **123**.

25   R. Jain, N. Jordan, D. Schild, E. D. van Hullebusch, S. Weiss, C. Franzen, F. Farges, R. Hübner and P. N. L. Lens, *Chem. Eng. J.*, 2015, **260**, 855–863.

26   D. K. Villa-Gomez, S. Papirio, E. D. van Hullebusch, F. Farges, S. Nikitenko, H. Kramer and P. N. L. Lens, *Bioresour. Technol.*, 2012, **110**, 26–34.

27   G. Xi, K. Xiong, Q. Zhao, R. Zhang, H. Zhang and Y. Qian, *Cryst. Growth Des.*, 2006, **6**, 577–582.

28   Z. He, Z. G. Wang, H. Y. Zhu, X. R. Liu, J. P. Peng and S. M. Hong, *Appl. Phys. Lett.*, 2014, **105**, 11901–5.

29   V. V Poborchii, A. V Kolobov and K. Tanaka, *Appl. Phys. Lett.*, 2014, **1167**, 22–25.

30   S. N. Yannopoulos and K. S. Andrikopoulos, *J. Chem. Phys.*, 2004, **121**, 4747–4758.

31   K. Yang, Q. Cui, Y. Hou, B. Liu, Q. Zhou, J. Hu, H.-K. Mao and G. Zou, *J. Phys. Condens. Matter*, 2007, **19**, 425220.

32   B. Gates, B. Mayers, B. Cattle and Y. Xia, *Adv. Funct. Mater.*, 2002, **12**, 219–227.

33   R. C. Dai, L. B. Luo, Z. M. Zhang and Z. J. Ding, *Mater. Res. Bull.*, 2011, **46**, 250–354.

34   A. Fernández-Martínez and L. Charlet, *Rev. Environ. Sci. Biotechnol.*, 2009, **8**, 81–110.

35   S. K. Mehta, S. Chaudhary, S. Kumar, K. K. Bhasin, K. Torigoe, H. Sakai and M. Abe, *Nanotechnology*, 2008, **19**, 295601.

36   R. S. Oremland, M. J. Herbel, J. S. Blum, S. Langley, T. J. Beveridge, P. M. Ajayan, T. Sutto, A. V Ellis and S. Curran, *Appl. Environ. Microbiol.*, 2004, **70**, 52–60.

37   T. Scopigno, W. Steurer, S. N. Yannopoulos, a Chrissanthopoulos, M. Krisch, G. Ruocco and T. Wagner, *Nat. Commun.*, 2011, **2**, 195.

38   Y. Qi, T. Xia, Y. Li, L. Duan and W. Chen, *Environ. Sci. Nano*, 2016, 1062–1071.

39   A. D. Lemly, *Aquat. Toxicol.*, 2002, **57**, 39–49.

40   T. S. Presser and S. N. Luoma, *Integr. Environ. Assess. Manag.*, 2010, **6**, 685–710.

1
2
3
4
5
6
7
8
9
10
11
12
13
14
15
16
17
18
19
20
21
22
23
24
25
26
27
28
29
30
31
32
33
34
35
36
37
38
39
40
41
42
43
44
45
46
47
48
49
50
51
52
53
54
55
56
57
58
59
60

1
2
3
4
5
6
7
8
9
10
11
12
13
14
15
16
17
18
19
20
21
22
23
24
25
26
27
28
29
30
31
32
33
34
35
36
37
38
39
40
41
42
43
44
45
46
47
48
49
50
51
52
53
54
55
56
57
58
59
60

41   M. Lenz, B. Kolvenbach, B. Gygax, S. Moes and P. F. X. Corvini, *Appl. Environ. Microbiol.*, 2011, **77**, 4676–80.

42   J. Tourney and B. T. Ngwenya, *Chem. Geol.*, 2014, **386**, 115–132.

FOOTNOTE

The SI contains extra figures with experimental data as noted in the text.

Shape change of biogenic elemental selenium nanoparticles decreases their colloidal stability

Rohan Jain[1*], Norbert Jordan[2], Satoru Tsushima[2], René Hübner[3],
Stephan Weiss[2], Piet Lens[1,4]

[1]*Department of Chemistry and Bioengineering, Tampere University of Technology,*

Korkeakoulunkatu 10, FI-33720 Tampere, Finland

[2]*Helmholtz-Zentrum Dresden - Rossendorf, Institute of Resource Ecology, Bautzner*

Landstraße 400, 01328 Dresden, Germany

[3]*Helmholtz-Zentrum Dresden - Rossendorf, Institute of Ion Beam Physics and Materials*

Research, Bautzner Landstraße 400, 01328 Dresden, Germany

[4]*UNESCO-IHE, Institute for Water Education, Westvest 7, 2611AX Delft, The Netherlands*

Corresponding author:

Phone: +358 401981098, e-mail: rohanjain.iitd@gmail.com, mailto: Department of

Chemistry and Bioengineering, Tampere University of Technology, Korkeakoulunkatu 10,
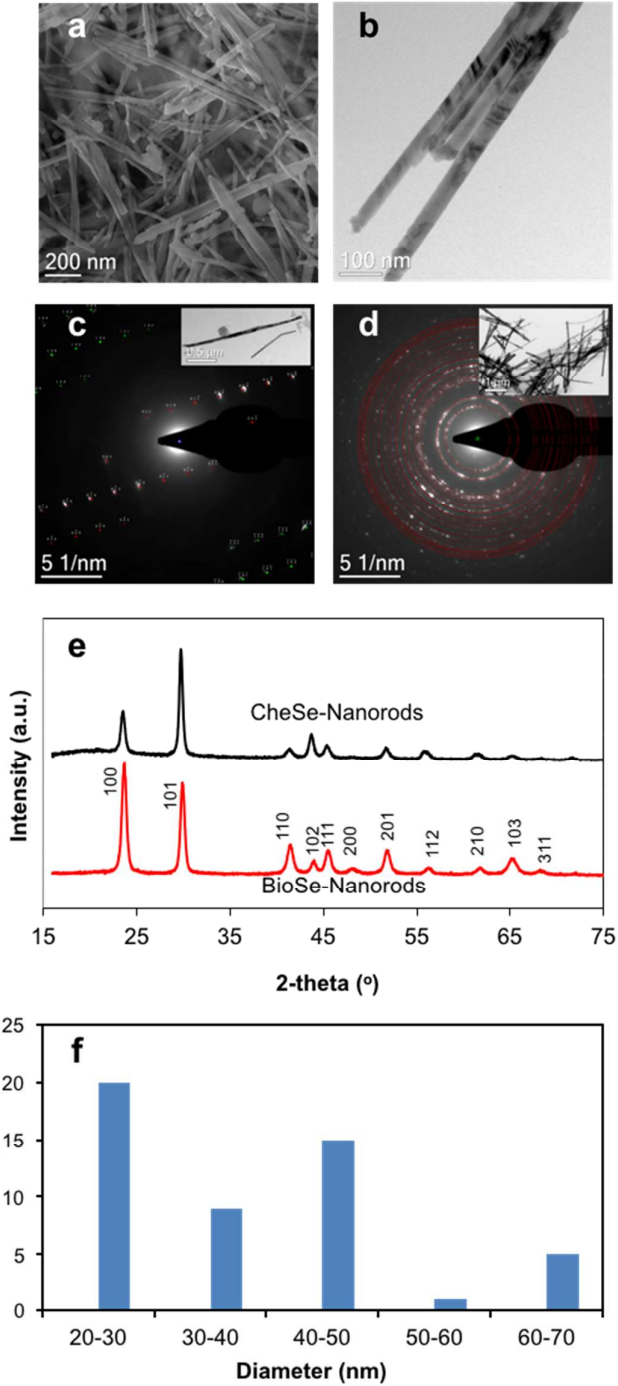
FI-33720 Tampere, Finland

1

Figure S1. (a) SEM and (b) TEM of purified BioSe-Nanorods after 120 h of incubation. SAED patterns of the purified, (c) single-crystalline BioSe-Nanorod (inset) and (d) multiple CheSe-Nanorods (inset) and their corresponding (e) XRD patterns. (f) Diameter distribution of BioSe-Nanorods based on SEM images.
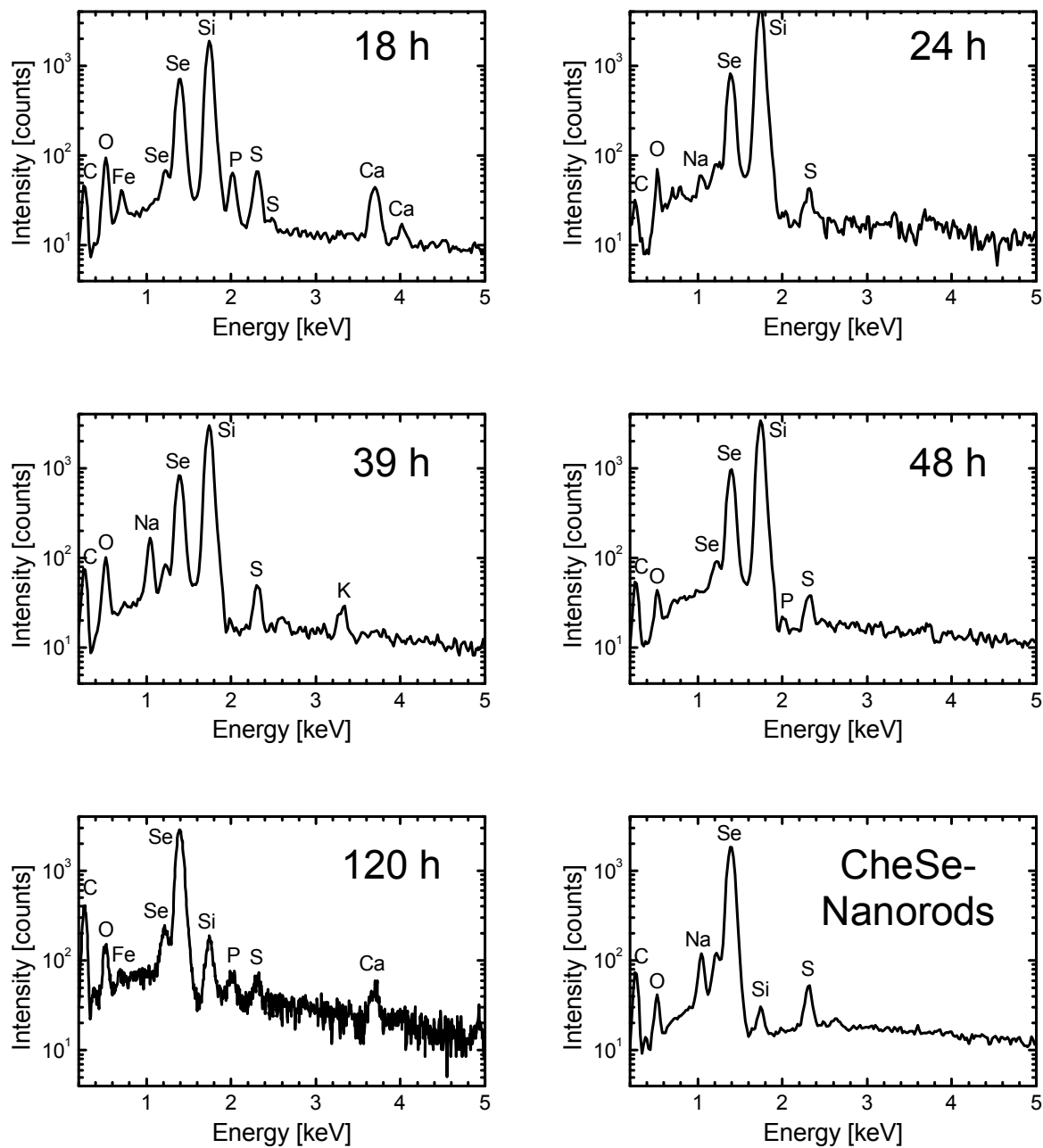
Figure S2. Energy-disperse X-ray spectra obtained in the SEM during the formation of BioSe-Nanorods after incubation of 18 h, 24 h, 39 h, 48 h and 120 as well as of CheSe-Nanorods.